Role of cerebellar GABAergic dysfunctions in the origins of essential tremor

Xu Zhang[a,b,c] and Sabato Santaniello[a,b,c,1]

[a]Biomedical Engineering Department, University of Connecticut, Storrs, CT 06269; [b]The Connecticut Institute for the Brain and Cognitive Sciences, University of Connecticut, Storrs, CT 06269; and [c]Brain Imaging Research Center, University of Connecticut, Storrs, CT 06269

Edited by Terrence J. Sejnowski, Salk Institute for Biological Studies, La Jolla, CA, and approved May 21, 2019 (received for review October 13, 2018)

Essential tremor (ET) is among the most prevalent movement disorders, but its origins are elusive. The inferior olivary nucleus (ION) has been hypothesized as the prime generator of tremor because of the pacemaker properties of ION neurons, but structural and functional changes in ION are unlikely under ET. Abnormalities have instead been reported in the cerebello-thalamo-cortical network, including dysfunctions of the GABAergic projections from the cerebellar cortex to the dentate nucleus. It remains unclear, though, how tremor would relate to a dysfunction of cerebellar connectivity. To address this question, we built a computational model of the cortico-cerebello-thalamo-cortical loop. We simulated the effects of a progressive loss of $GABA_A$ α_1-receptor subunits and up-regulation of $\alpha_{2/3}$-receptor subunits in the dentate nucleus, and correspondingly, we studied the evolution of the firing patterns along the loop. The model closely reproduced experimental evidence for each structure in the loop. It showed that an alteration of amplitudes and decay times of the GABAergic currents to the dentate nucleus can facilitate sustained oscillatory activity at tremor frequency throughout the network as well as a robust bursting activity in the thalamus, which is consistent with observations of thalamic tremor cells in ET patients. Tremor-related oscillations initiated in small neural populations and spread to a larger network as the synaptic dysfunction increased, while thalamic high-frequency stimulation suppressed tremor-related activity in thalamus but increased the oscillation frequency in the olivocerebellar loop. These results suggest a mechanism for tremor generation under cerebellar dysfunction, which may explain the origin of ET.

essential tremor | Purkinje cells | dentate nucleus | inferior olivary nucleus | GABA

Essential tremor (ET) is a progressive neurological disease and among the most prevalent movement disorders (1). ET is characterized by a 4- to 12-Hz kinetic tremor that occurs in the upper limbs and may eventually spread to the neck and jaws, or accompany gait symptoms (2, 3). Clinically, only ∼50% of the ET patients receive benefits from medications, while for the rest of the population, deep brain stimulation (DBS) of the ventral intermediate thalamus (Vim) is the main alternative therapy (4). Despite large interest, the origins of ET remain unclear. It has been hypothesized that tremor has a central origin in the brainstem (5), where pacemaker neurons with prominent subthreshold oscillations in the range of ET frequencies have been identified in the inferior olivary nucleus (ION) (6, 7). Further evidence in support of this hypothesis has been provided by animal studies involving the injection of the neurotoxin harmaline (8, 9), which primarily targets ION neurons and causes generalized kinetic tremor. However, no consistent structural or functional change has been observed in the ION of ET patients compared with healthy controls (10–12). Evidence suggests, instead, that ET is associated with microstructural changes and neuronal dysfunctions in the cerebellum (13–15) including a loss of dendritic spines in Purkinje cells in the cerebellar cortex, a decrease in $GABA_A$ and $GABA_B$ receptors in the dentate nucleus, and a deficit of bound GABA transmitters (16–19). These changes have been correlated with the tremor severity (13) and may lead to significant alterations in the motor network (20, 21). It remains unclear, though, how these changes may relate to tremor.

Studies involving genetically modified mice (22, 23) have shown that the deletion of $GABA_A$ receptor α_1 subunits results in the loss of 50% of all $GABA_A$ receptors in the cerebellar structures and that such deletion is associated with kinetic tremor and motor incoordination, which are both characteristics of ET. Furthermore, it has been reported that the loss of α_1 subunits is partially compensated by an overexpression of α_2 and α_3 subunits (23, 24), which colocalize with the α_1 subunits in the cerebellar nuclei and the molecular layer of the cerebellar cortex in rodents as well as humans (25, 26) and are responsible for longer opening of ion channels and slowly decaying synaptic currents (27–29). Finally, an increase of tonic $GABA_A$ receptor-mediated currents has been reported in case of loss of α_1 subunits (30). Altogether, these studies indicate that a substantial modulation of the temporal dynamics of the GABAergic currents may occur in the cerebellum under ET condition.

Here we constructed a computational model of the cortico-cerebello-thalamo-cortical (CCTC) loop and investigated whether changes to the dynamics of the GABAergic currents to the dentate nucleus may elicit tremor-related neuronal activity along the CCTC loop. The model includes single-compartment neurons from the brainstem (ION), the cerebellum (dentate nucleus and cerebellar cortex), the Vim, and the motor cortex (MC) according to a network topology derived from the primates' anatomy. The model reproduces the average firing rates and discharge patterns

Significance

We investigated the mechanisms of tremor generation in essential tremor (ET). Using computational modeling we show that tremor-related activity can originate from the olivocerebellar loop in response to a dysfunction and compensatory up-regulation of GABA receptors in the dentate nucleus of cerebellum. The emerging tremor-related activity then projects to thalamus and reaches the corticothalamic motor loop. Consistent with clinical observations, the study shows that the tremor frequency decreases as the up-regulation becomes stronger and increases as high-frequency stimulation is delivered to the thalamus. Our results provide an explanation of how local synaptic abnormalities would lead to widespread tremor-related neural activity in ET and suggest that compensatory processes in degenerative diseases may underlie brain dysfunction.

Author contributions: X.Z. and S.S. designed research; X.Z. performed research; X.Z. analyzed data; and X.Z. and S.S. wrote the paper.

The authors declare no conflict of interest.

This article is a PNAS Direct Submission.

[1]To whom correspondence may be addressed. Email: sabato.santaniello@uconn.edu.

This article contains supporting information online at www.pnas.org/lookup/suppl/doi:10.1073/pnas.1817689116/-/DCSupplemental.

Published online June 17, 2019.

of single units in nonhuman primates and mice under normal conditions as well as tremor conditions for all modeled structures, where the recordings under tremor conditions were derived from animal studies involving the neurotoxin harmaline.

We show through numerical simulations that a progressive combination of reduced synaptic conductance and prolonged decay of the GABAergic currents in the synapses between Purkinje cells and deep cerebellar neurons may facilitate sustained oscillatory activity at the frequency of tremor in the olivocerebellar loop, i.e., ION, cerebellar cortex, and dentate nucleus. The oscillations propagate to the thalamocortical system (Vim-MC) and induce a sustained bursting activity in the Vim with characteristics that are consistent with the activity of tremor cells in ET patients (31, 32). Consistent with clinical observations (33, 34), the frequency of the oscillatory activity slowly decreases by ~1 Hz as the manipulation of GABAergic currents progresses and is instead increased by about 0.4 Hz when electrical stimulation at the frequency of therapeutic DBS (185 Hz) is applied to Vim. DBS also reduces the range of GABAergic settings that can sustain tremor-related oscillations, thus suggesting that even though primarily targeting the thalamocortical system, thalamic DBS may exert secondary effects on the olivocerebellar loop in ET patients. Finally, we show that neural oscillations leading to tremor-related bursting activity in the Vim can originate from a localized perturbation applied to a small portion of olivary neurons and spread through the entire cortico-olivo-cerebellar network, which further indicates the robustness of tremor-related neural dynamics and supports a possible network origin for ET.

Results

The CCTC network model (Fig. 1*A*) includes (*i*) the olivocerebellar loop, including eight ION neurons in the brainstem (*SI Appendix*, Fig. S1 *A–D*), 40 Purkinje cells (PC) and four granular layer clusters (GrL) in the cerebellar cortex (each GrL cluster includes one granule cell, one Golgi cell, and one stellate cell), and one glutamatergic deep cerebellar projection neuron (DCN) and one nucleoolivary neuron (NO) in the dentate nucleus (*SI Appendix*, Fig. S1 *E–H*); (*ii*) the thalamocortical system, including the Vim [1 thalamocortical neuron (TC)] and the MC (20 pyramidal neurons [PYN] and two fast-spiking interneurons [FSI]), (*SI Appendix*, Table S1). The connections between different neuron types are modeled using conductance-based synapses (*SI Appendix*, Table S2) and were constrained to reproduce the neuronal activity observed in vivo in PCs and DCN from healthy nonhuman primates during voluntary arm movements (*SI Appendix*, Fig. S2) (35). The connection graphs are reported in *SI Appendix*, Fig. S3, and were determined to be consistent with the neuronal anatomy in humans and animal models as these structures are largely conserved across species (36). The relay functions of the red nucleus (RN) along the dentato-rubro-olivary pathway (37–39) and of the pontine nuclei (PN) along the cortico-ponto-cerebellar pathway (40, 41), as well as the interneuron network (IN) in the cerebellar cortex (gray circles in Fig. 1*A*), are not explicitly modeled and are subsumed in the latency between presynaptic and postsynaptic structures (*SI Appendix*, *Note 1*).

Model Validation under Normal and Harmaline Conditions. In addition to reproducing the neuronal activity observed in vivo in Purkinje cells and deep cerebellar neurons from healthy nonhuman primates (*SI Appendix*, Fig. S2), the injected current parameters and synaptic gains in the CCTC loop were constrained such that the average firing rates of NO, TC, and PYN cells match the range of experimental values reported in refs. 31, 37, and 42 from in vivo recordings in healthy animals (NO, 5.5 ± 2.0 Hz; TC, 26.6 ± 4.2 Hz; PYN, 23.1 ± 5.0 Hz, mean ± SD; values estimated over 60,000-ms-long simulation).

Fig. 1 *B–E* shows the effects of the activation of ION neurons on the major projecting neurons in the cerebellum, i.e., PC and DCN, via climbing fibers. In response to ION activation, the PC exhibits a complex of spikes with amplitude and frequency modulation (Fig. 1 *B*, *Inset*), where the shape and duration of

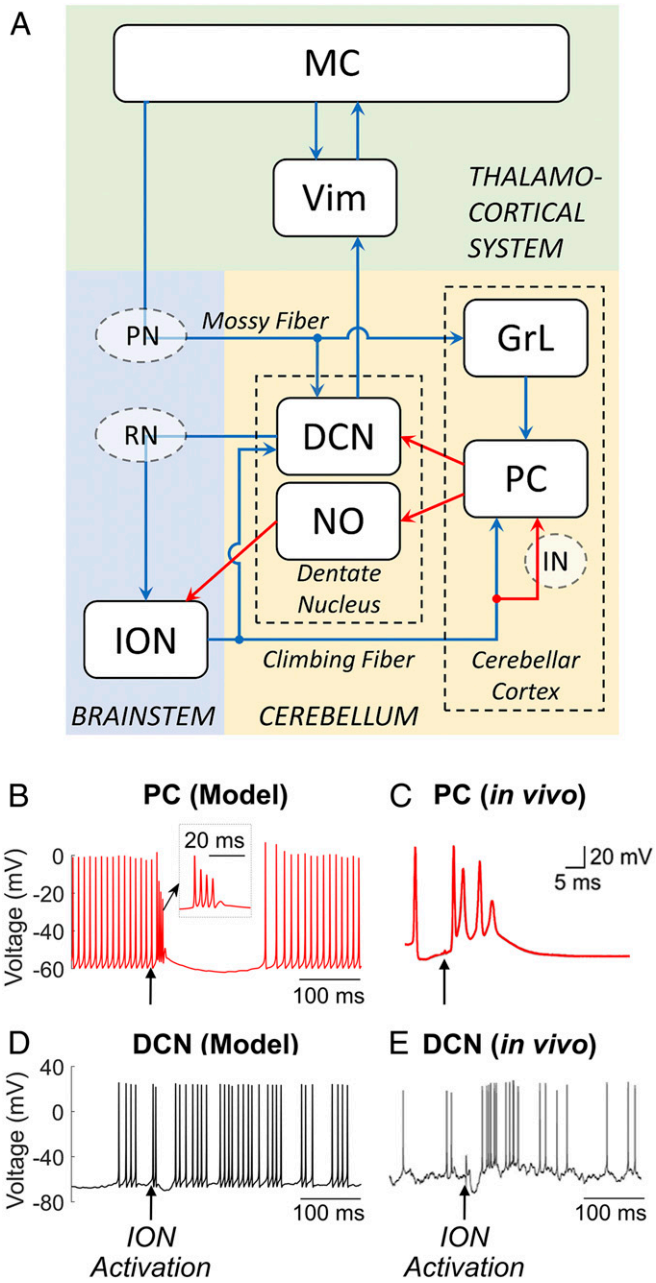

Fig. 1. (*A*) Schematic of the CCTC model. Blue arrows, glutamatergic excitatory connections; red arrows, GABAergic inhibitory connections; PC, Purkinje cells; DCN, deep cerebellar neurons; NO, nucleoolivary neurons; ION, inferior olive nucleus; GrL, granular layer; RN, red nucleus; PN, pontine nucleus; IN, cerebellar interneurons; Vim, ventral intermediate nucleus of the thalamus; MC, motor cortex. (*B–E*) Response of PC and DCN neurons to a depolarizing stimulus applied in the ION in the proposed network model (*B* and *D*) and in rodents in vivo (*C* and *E*) in normal, tremor-free conditions. A single suprathreshold (10 pA) current pulse (pulse duration of 20 ms) was applied to all ION neurons in our model (black arrows in *B* and *D*) and in the inferior olivary nucleus of the rodent (black arrows in *C* and *E*) and resulted in a burst of action potentials with amplitude adaptation (i.e., complex spike) in the PC (*B* and *C*) and an after-hyperpolarization rebound burst of action potentials in the DCN (*D* and *E*). (*B*, *Inset*) Zoom-in of the complex spike. Image in *C* is reprinted from ref. 43, which is licensed under CC BY 3.0. Image in *E* is reprinted from ref. 45, which is licensed under CC BY 4.0.

spikes matched experimental recordings from rodents (43) (Fig. 1 *B* and *C*). The PC then presents a long pause after the complex spike, which is consistent with data reported in ref. 44. The PC complex spiking contributes to the hyperpolarization of the DCN in the dentate nucleus and the consequent formation of rebound bursts, which are consistent with data in refs. 45 and 46 (Fig. 1 *D* and *E*).

When simulated under normal condition, the TC neuron in the Vim spikes irregularly (Fig. 2*G*) as reported in ref (31). While the ION neurons exhibit subthreshold oscillations at 5.6 Hz, which are well aligned with in vivo recordings from rodents (47, 48). The rare occurrence of spikes in the ION neurons (Fig. 2*A*) reflects the fact that ION neurons mainly respond to sensory stimuli, while their probability of spiking becomes minimal during movements (49, 50).

To verify that the CCTC model is able to reproduce the experimental tremor conditions induced by harmaline, we simulated the localized effects of the neurotoxin harmaline on the ION neurons by potentiating the calcium channels as in ref. 6 (*Materials and Methods*). The direct effect of this change is a spontaneous synchronous firing of the ION neurons at 7.1 Hz (tremor frequency), consistent with the frequency of harmaline tremor in the primate model (51). We tracked the effects of the ION synchronous firing on the network, and we confirmed a periodic bursting pattern in the Vim (burst duration, 102.1 ± 15.0 ms; mean burst frequency, 7.1 Hz across three instances of the CCTC model) (Fig. 2*H*). Accordingly, the power spectral density of the Vim showed a strong peak at the tremor frequency and followed the spectrum of tremor cells recorded in ET patients in vivo (31) (Fig. 2 *I* and *J*).

The mechanism of propagation of the oscillations from the ION to the Vim depends on a significant shift in the discharge pattern of the PCs and the DCN associated with these oscillations: the PCs shift from tonic firing with occasional complex spikes and pauses (Fig. 2*C*) to periodic complex spikes (Fig. 2*D*) driven by the sustained ION activation (Fig. 2*B*) through the climbing fibers, while the DCN transitions from irregular firing to sequences of rebound bursts at the tremor frequency (burst duration, 109.4 ± 9.7 ms; interburst intervals, 30.3 ± 4.6 ms; mean ± SD) (Fig. 2 *E* and *F*). Overall, these results indicate that the olivocerebellar (ION→PC→DCN) pathway can facilitate the propagation of oscillations within the tremor frequency band (4–12 Hz) toward the thalamocortical system.

GABAergic Dysfunction in the DCN Facilitates Olivocerebellar Oscillations. To explore the relationship between cerebellar GABAergic dysfunctions and the possible origins of ET, we simulated the concurrent loss of $GABA_A$ α_1-receptor subunits and up-regulation of α_2/α_3-receptor subunits in the cerebellum by progressively lowering the maximum synaptic conductance $g_{PC\to DCN}$ and increasing the decay time $\tau^{PC\to DCN}$ of the synaptic currents from PCs to DCN (range, 2–24 ms; nominal value under normal conditions, 2.4 ms; *SI Appendix*, *Note 1* and Table S2). The effect of these changes was a progressive modulation of the shape and duration of the synaptic currents, which span the range reported in vitro (28, 30, 52) that goes from the normal composition of α_1-receptor subunits to the complete dominance of α_2/α_3-receptor subunits. The GABAergic currents to NO, instead, were not altered because they are significantly smaller than the currents to DCN (53) and mainly mediated by α_3-receptor subunits (54), which make these currents more than 10-fold slower than the currents to DCN (see $\tau^{PC\to NO}$ in *SI Appendix*, Table S2) and less likely to be affected by ET.

Fig. 3*A* reports the range of values tested for $\tau^{PC\to DCN}$ and the ratio R between the synaptic gains $g_{PC\to DCN}$ and $g^*_{PC\to DCN}$, where $g^*_{PC\to DCN}$ is the nominal conductance value under normal conditions. An initial perturbation consisting of a single 20-ms-long depolarizing current pulse (10 pA) was delivered at time t =

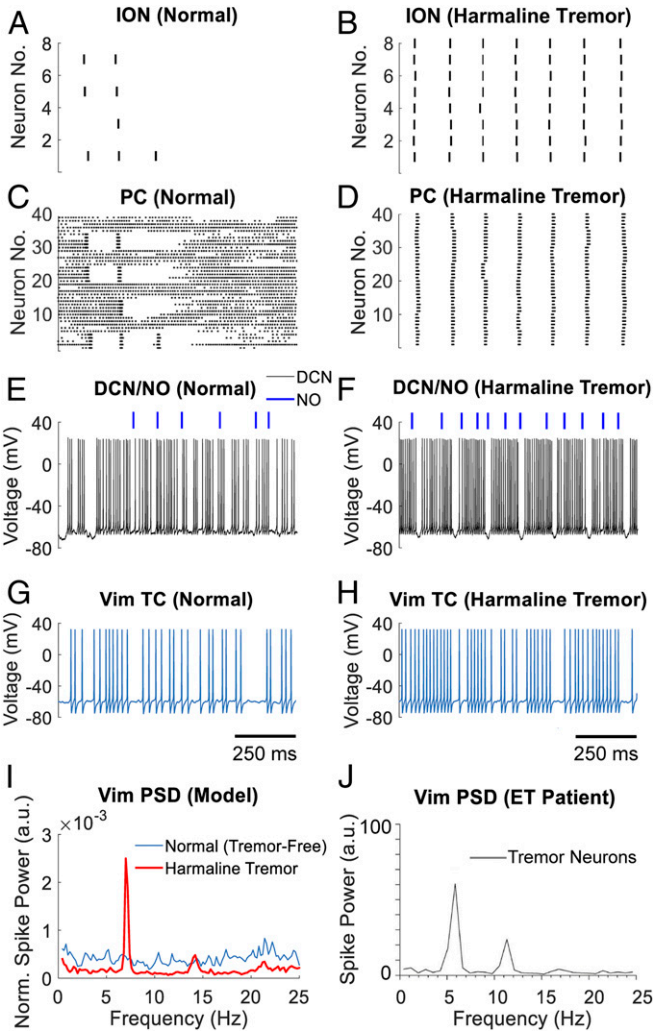

Fig. 2. Single unit activity of neurons in the CCTC model under normal and harmaline-induced tremor conditions. (*A–H*) Raster plot of ION neurons and PCs under normal condition (*A* and *C*) and harmaline-induced tremor condition (*B* and *D*), respectively, and correspondent membrane voltage of the DCN and TC neurons (*E* and *G*, normal condition; *F* and *H*, tremor condition, respectively). Blue bars in *E* and *F* report the timing of action potentials fired by the NO neuron. Data in *A–H* are from one instance of the CCTC model simulated over a 4,000-ms-long period. Time scales in *G* and *H* also apply to *A*, *C*, and *E* and *B*, *D*, and *F*, respectively. (*I* and *J*) Comparison between the power spectral density (PSD) of the TC neuron in the CCTC model and a tremor cell in the Vim of an ET patient, respectively. PSD in *I* is reported under normal tremor-free (blue curve) and harmaline-induced tremor conditions (red curve). PSD curves are averaged across three instances of the CCTC model, each one simulated over a 60,000-ms-long period. PSD in *J* is reported for a single tremor cell in a patient with ET. Image in *J* is reprinted with permission from ref. 31.

1,000 ms to the ION neurons to mimic a transient exogenous stimulus from afferent projections (*SI Appendix*, Fig. S4). The spiking activity of the ION neurons and the Vim PSD were monitored in the following 3,000 ms. The region with tremor was defined as the parameter combinations (R, $\tau^{PC\to DCN}$) for which any ION neuron sustained spiking for >2,000 ms after an initial perturbation. Correspondingly, the power spectrum of the Vim was inspected, and the peak frequency (i.e., the frequency of peak PSD value) was used as a proxy of the tremor activity if within the band 4–12 Hz.

As reported in Fig. 3*A*, the range of ratios R that can sustain tremor activity increases with longer $\tau^{PC\to DCN}$. Moreover, as the

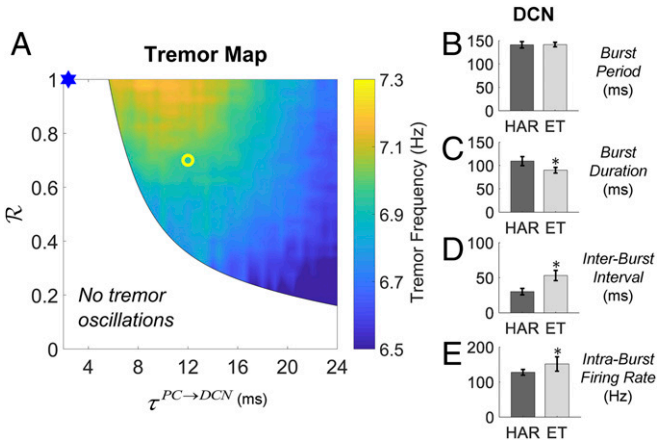

Fig. 3. Effects of cerebellar GABAergic dysfunctions on tremor-related neural oscillations in the CCTC model. (*A*) Two-dimensional map depicting the region of the parameter space (R, $\tau^{PC\rightarrow DCN}$) where tremor activity in the Vim is observed along with the tremor peak frequency. The blue mark indicates parameters used to simulate normal, tremor-free conditions. The yellow circle indicates parameters used for the ET-like tremor activity analyzed in *B* and *E*, i.e., R = 0.7, $\tau^{PC\rightarrow DCN}$ = 12 ms. For each combination of parameters (R, $\tau^{PC\rightarrow DCN}$), the CCTC model was simulated for 4,000 ms, and the first 1,000 ms were excluded from subsequent analyses. (*B–E*) Comparison between the bursting activity of DCN under harmaline-induced tremor (HAR; black bars) and GABAergic dysfunctions of the PC-DCN synapses (ET; gray bars). The burst analysis was performed as reported in *SI Appendix, Note 2*, on data collected over 60,000-ms-long simulations. The average burst period (*B*), burst duration (*C*), interburst interval (*D*), and intraburst discharge rate (*E*) are reported as mean ± SD across three model instances. Asterisks denote significant difference (Wilcoxon rank-sum test, $P < 0.01$) between values measured under HAR and ET conditions.

pair (R, $\tau^{PC\rightarrow DCN}$) moves toward the lower right quadrant of Fig. 3*A* (i.e., further degeneration of the GABAergic currents), the frequency of tremor decreases by ∼1 Hz, thus showing a progressive adjustment that matches longitudinal observations reported in ET patients (33, 34). We also assessed the role of the NO in forming tremor-related network oscillations. Specifically, we repeated the simulations in Fig. 3*A* with the synaptic strength of the NO→ION projection decreased by 50%. The results are reported in *SI Appendix*, Fig. S5, and indicate that the tremor region is enlarged when the NO neuron exerts less inhibitory input into the ION neurons, which suggests that the NO neurons may regulate the susceptibility of the network to enter into tremor-related oscillations.

As in the harmaline condition, the cerebellar GABAergic dysfunctions (denoted here as "ET condition") were associated with a tonic synchronous spiking of the ION neurons, which led to the Vim activity in the tremor band 4–12 Hz. Differently from the harmaline condition, though, a significant change of the bursting pattern was observed in the discharge pattern of the DCN. Fig. 3 *B–E* report the burst analyses for the DCN under harmaline and one ET condition (yellow circle in Fig. 3*A*). Although in both cases the ION neurons spiked synchronously and DCN exhibited similar bursting frequencies (Fig. 3*B*), the DCN fired shorter bursts with higher intraburst rates and longer interburst intervals (Fig. 3 *C–E*) under ET condition, which reflect a prolonged periodic presynaptic inhibition (see *SI Appendix*, Fig. S4, for the behavior of other structures). Note that the ET condition was obtained with no manipulation of the properties of the ION neurons. This indicates that a manipulation of the bidirectional interaction between the ION and the cerebellar structures, which is secondary to the cerebellar GABAergic dysfunctions, can enable and facilitate widespread network oscillations that would ultimately lead to the tremulous activity in the Vim.

Phase-Dependent Excitation of ION Neurons Underlies Persistent Network Oscillations. To determine the mechanism of tremor generation in ET, we focused on the disynaptic excitatory pathway from DCN to ION neurons, i.e., the dentato-rubro-olivary projection. Since it has been indicated that ION neurons spike in response to exogenous depolarizing stimuli at a preferred phase of the subthreshold membrane voltage oscillation (48), we isolated the ION model and controlled the timing of the input to the ION neurons by delivering a suprathreshold depolarizing current pulse to all ION neurons at a specific onset time *T* after the last ION spike. We varied both the amplitude of the pulse (I_{STEP}, range: 0–1.0 pA, which is comparable to the range of synaptic input from DCN) and *T* (up to 175 ms, which is approximately the subthreshold oscillation period of ION). The pulse was kept on till any of the eight ION neurons fired an action potential (Fig. 4*A*, red curve), in which case the stimulus was then turned off and reapplied with the same onset *T* after the new ION neuron's spike. Accordingly, the ION neurons received a train of current pulses with the same amplitude and time-varying durations, all delivered at approximately the same phase of their subthreshold oscillation. If the current pulse did not trigger another spike from any ION neuron until the end of the subthreshold oscillation cycle (Fig. 4*A*, black curve), then that specific parameter pair (I_{STEP}, *T*) would be labeled as unable to trigger ION spiking. Fig. 4*B* shows that stimuli delivered at earlier phases of the subthreshold oscillation, e.g., $T < 50$ ms, would hardly trigger ION spiking and would therefore prevent the olivocerebellar system to engage in tremor-related oscillations (Fig. 4*B*, gray background). Stimuli delivered at a later onset, instead, robustly sustained ION spiking, and the frequency of the spikes depends on both the pulse intensity I_{STEP} and the specific onset *T*. Furthermore, as shown in Fig. 4*C*, the average ION firing rate increases with the pulse intensity I_{STEP}, but the relationship between the pulse duration, which is related to the pulse onset, and the firing rate is nonlinear, with the highest ION firing rate occurring for pulse durations in the range 60–80 ms. This indicates that the ION neurons are highly selective against the timing of the input excitation and that the ION spiking is most efficiently triggered by inputs arriving at a specific timing.

Finally, for each pair (R, $\tau^{PC\rightarrow DCN}$), we compared the predictions of the isolated ION model in Fig. 4*B* to the net synaptic input delivered from DCN to ION neurons via RN in the full CCTC model. We measured the average lag between the onset of each DCN burst and the onset of the ION action potential that precedes it (i.e., $\Delta_{ION\rightarrow DCN\_burst}$ in Fig. 4*D*). As shown in Fig. 4*E*, 91.8% of the pairs (904 out of 985) that resulted in tremor at the Vim had $\Delta_{ION\rightarrow DCN\_burst} > 50$ ms, which is consistent with the map in Fig. 4*B* for sustained ION spiking. Similarly, in 85.4% of the pairs (696 out of 815) in the tremor-free region (white area in Fig. 3*A*), the average $\Delta_{ION\rightarrow DCN\_burst}$ was below 50 ms. Altogether, these results indicate that the changes in the shape of the GABAergic currents may facilitate the generation of sustained spiking in the ION neurons at tremor frequencies by modulating the duration and rate of the bursting activity of DCN, which activated the ION neurons robustly through the dentato-rubro-olivary pathway (RN pathway in Fig. 4 *D*, *a*).

To further elucidate the tremor generation mechanism, Fig. 4*D* reports the timing of action potentials in ION, PC, and DCN neurons under normal (Fig. 4 *D*, *b*, *d*, and *f*) and ET conditions (Fig. 4 *D*, *c*, *e*, and *g*). Under normal conditions, the short interburst interval of the DCN is inefficient in activating the ION. In presence of GABAergic dysfunctions to the PC–DCN connection, instead, the olivary activation can cause a prolonged hyperpolarization of the DCN, which is followed by a rebound burst that is in resonance with the ION subthreshold oscillatory

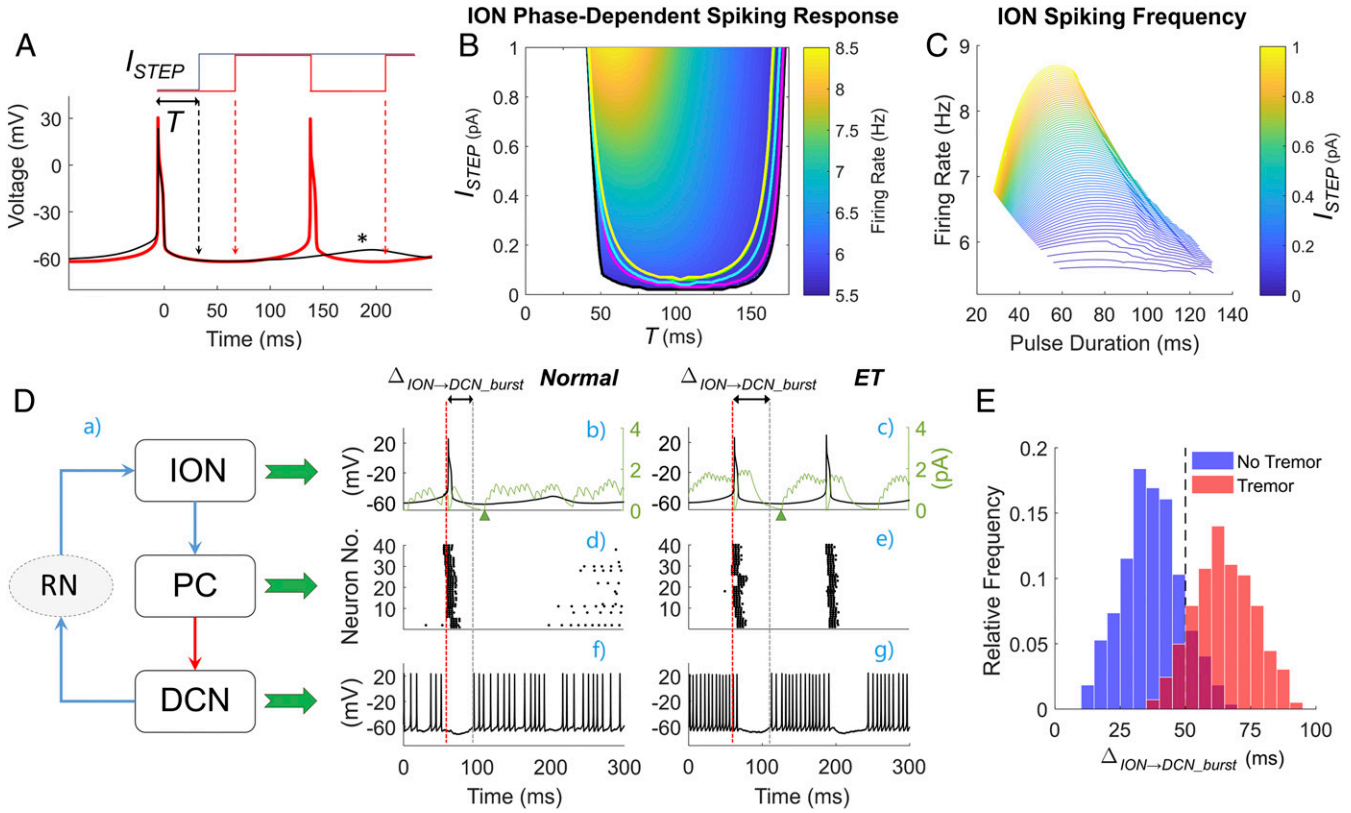

Fig. 4. Role of the phase of ION subthreshold oscillations in the generation of tremor-related network oscillations. (*A*) In any ION neuron, the lag between an action potential and the peak of the following subthrehsold oscillation (black asterisk) defines the duration of the oscillation cycle. The onset time *T* of the depolarizing input current I_{STEP} is varied between 0 (i.e., at the time of the action potential) and the peak of the subthreshold oscillation. The current is transiently turned off when an action potential is generated (red line). (*B*) Two-dimensional map depicting the region of the parameter space (I_{STEP}, *T*) where ION neurons sustain tonic spiking along with the resultant firing rate. Curves in black, pink, cyan, green, and yellow denote the region where at least 4, 5, 6, 7, or all ION neurons sustain spiking simultaneously, respectively. For each combination (I_{STEP}, *T*) in *B*, three model instances were simulated over a 4,000-ms-long period, and the simulation results from the first 1,000 ms were discarded. The firing rate was measured from any ION neuron that sustained spiking until the end of simulation. (*C*) The ION firing rate as a function of the duration of the current I_{STEP} for several values of the current intensity. (*D*) Role of the dentato-rubro-olivary pathway in propagating tremor-related oscillations through the olivocerebellar loop. A schematic of the interconnections between ION, PC, and DCN cells mediated by disynaptic connections through the red nucleus (RN) is provided (*a*) along with the simulated spiking activity of an ION neuron (black lines; *b* and *c*), PCs (*d* and *e*), and the DCN (*f* and *g*) under normal, tremor-free condition (*b*, *d*, and *f*) and ET condition (i.e., yellow circle in Fig. 3*A*) (*c*, *e*, and *g*). Green lines in *b* and *c* denote the postsynaptic glutammatergic currents to the ION neuron mediated by the RN. The red vertical lines denote the onset time for the ION neuron's action potential. This action potential elicits a complex spike in the PCs, which hyperpolarizes the DCN and causes a post-hyperpolarization rebound burst (*f* and *g*). The lag $\Delta_{ION\rightarrow DCN\_burst}$ between the ION neuron's action potential and the DCN rebound predicts whether the ION neuron will spike again and corresponds to the parameter *T* in *A* and *B*. Time scales in *f* and *g* also apply to *b* and *d* and to *c* and *e*, respectively. (*E*) Histogram of the values of $\Delta_{ION\rightarrow DCN\_burst}$ measured under nontremor (blue bars) and ET conditions (red bars). For each condition, data were obtained from the simulations reported in Fig. 3*A*.

activity. The glutamatergic postsynaptic currents elicited by the DCN activity via the RN pathway (Fig. 4 *D*, *b* and *c*) can therefore effectively trigger recurrent ION spikes.

Therapeutic Vim DBS Enhances the Frequency of Network Oscillations. High-frequency (150–185 Hz) DBS of the Vim is clinically recognized for the treatment of essential tremor (55). Although effective at reducing the amplitude of the tremor, Vim DBS is known to alter secondary pathophysiologic characteristics of ET, including tremor frequency and regularity, without restoring these characteristics to normal conditions (34, 56). Accordingly, we investigated the effects of Vim DBS at 185 Hz on the oscillatory activity in the olivocerebellar loop for every pair (R, $\tau^{PC\rightarrow DCN}$) considered in Fig. 3*A*. DBS was simulated as a train of square current pulses (pulse width, 0.2 ms) whose amplitude (10 nA) was chosen to be subthreshold to elicit tonic firing activity in the Vim (average rate, 92.6 ± 0.5 Hz, mean ± SD) and to suppress the tremor peak in the Vim power spectral density as in ref. 57 for all pairs (R, $\tau^{PC\rightarrow DCN}$) (Fig. 5*A*).

Despite suppressing the bursting activity in the Vim, the ION and DCN neurons continued to spike and burst, respectively, at the tremor frequency. The range of pairs (R, $\tau^{PC\rightarrow DCN}$) that resulted in sustained activity, though, was reduced by 18.8% compared with the case without DBS, while the spiking frequency of the ION neurons across all pairs (R, $\tau^{PC\rightarrow DCN}$) in the tremor region increased by 4.2 ± 3.9% (mean ± SD) (Fig. 5*B*). Furthermore, we analyzed the burstiness of the DCN for the pair of parameters (R, $\tau^{PC\rightarrow DCN}$) considered in Fig. 3 *B*–*E* (ET case), and we found that when 185-Hz Vim-DBS was applied, the length of the DCN interburst intervals decreased by 21.3 ± 14.8% (mean ± SD). Finally, we quantified the effects of the Vim DBS frequency on the olivocerebellar system by measuring the burstiness of the DCN patterns and the average ION firing rate as the DBS frequency varied from 2.5 to 185 Hz. We found that the average DCN interburst interval duration decreased as the DBS frequency increased (Fig. 5*C*) and the regularity of the DCN bursts increased (i.e., decreased coefficient of variation of the interburst durations; Fig. 5*C*, Inset), while the average ION

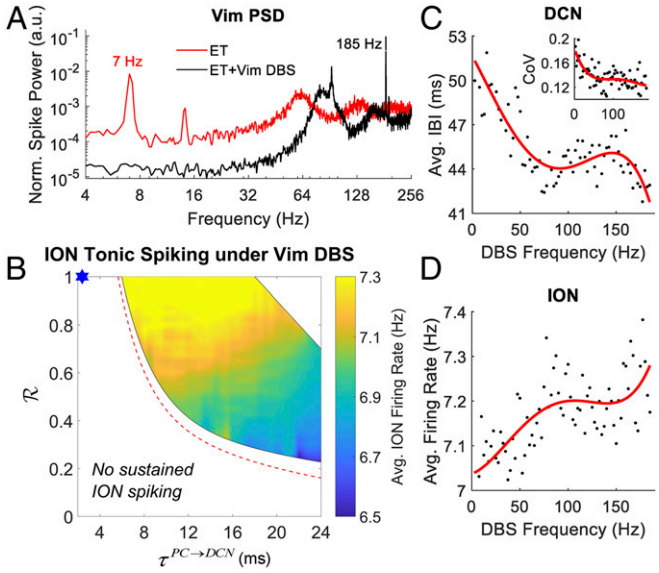

Fig. 5. Effect of Vim deep brain stimulation (DBS) under cerebellar GABAergic dysfunctions. (*A*) Power spectral density (PSD) of Vim under ET condition (i.e., yellow circle in Fig. 3A) with 185-Hz DBS of the Vim (ET + Vim DBS; black line) and without Vim DBS (ET; red line). Note the logarithmic scale on the axes. (*B*) Two-dimensional map depicting the region of the parameter space (R, $\tau^{PC\rightarrow DCN}$) where tonic spiking activity in the ION neurons is observed under 185-Hz DBS of the Vim along with the average ION firing rate. The red dashed lines indicate the boundary of the tremor region when no DBS was applied. The upper right region with no sustained ION firing is due to overly strong DCN rebound firing, which is facilitated as a result of DBS and is not compensated by the postsynaptic inhibitory currents elicited by the PC complex spikes. The PSD curves in *A* and the 2-D map in *B* are obtained from 4,000-ms simulations of the CCTC model (first 1,000 ms are discarded to let model instances reach steady-state conditions). (*C*) Average interburst interval (IBI) for the DCN in response to Vim DBS at different frequencies (black dots) and least-square fourth order polynomial fit (red curve, coefficient of determination for the fitting R^2= 0.73). (*Inset*) Coefficient of variation (CoV) of the IBI values under Vim DBS (black dots) and least-square fourth-order polynomial fit (red curve; R^2 = 0.41). (*D*) Average firing rate of the ION neurons under Vim DBS at different frequencies (black dots) and fourth-order polynomial fit (red curve; R^2 = 0.48). Each data point in *C* and *D* is obtained from a 5,000-ms simulation of the CCTC model (first 1,000 ms were discarded for initialization) under ET condition.

firing rate increased (Fig. 5*D*). Furthermore, both changes in ION and DCN activity became more stable for DBS frequencies above 100 Hz (plateau effect; Fig. 5 *C* and *D*).

Since no antidromic effect of DBS onto the cerebellothalamic pathway was included in our model, we hypothesized that the changes to the dentate nucleus and ION neurons were mediated by a modulation of the cortico-ponto-cerebellar pathway. *SI Appendix*, Fig. S6*A*, reports the average firing rate of the pyramidal neurons (PYN) as the DBS frequency increased from 0 Hz (i.e., no DBS) to 185 Hz, and it shows that the PYN firing rate grew linearly as the DBS frequency increased from 0 to 100 Hz and then plateaued at the DBS frequency range 100–185 Hz. The increase in the PYN firing rate was inversely correlated with the average DCN interburst interval duration (*SI Appendix*, Fig. S6*B*) and positively correlated with the average ION spiking rate (*SI Appendix*, Fig. S6*C*).

Altogether, these results indicate that while effective at masking the tremor activity in the thalamocortical system, Vim DBS does not eliminate tremor-related oscillatory activity in the olivocerebellar system. The DBS-mediated increment in cortical excitability, however, may counteract the prolonged hyperpolarization of the deep cerebellar neurons and therefore modulate the oscillations in the olivocerebellar system. These modulatory effects may explain the increased tremor frequency but reduced tremor intensity in ET patients under therapeutic Vim DBS (34).

Tremor Oscillations Could Spread Across Multiple Olivocerebellar Loops. To further assess the robustness of the tremor-related oscillations emerging in the olivocerebellar system under GABAergic dysfunction as the size and complexity of the CCTC loop increases, we expanded the original CCTC network by scaling up the number of neurons included in the model by a factor 5. The resultant scale-up CCTC model included 425 single-compartment neurons with similar ratios between neural populations. In addition, the interconnections between neurons in each population as well as the disynaptic projections between DCN and ION neurons were randomized to avoid the formation of local closed-loop circuits between neurons in the cerebellum and ION. See *SI Appendix*, *Note 3*, for details.

Under normal condition, an initial perturbation as described in *GABAergic Dysfunction in the DCN Facilitates Olivocerebellar Oscillations* was applied to all ION neurons (40 out of 40) simultaneously, but no ION neuron eventually engaged into tonic spiking activity, which led to no sustained oscillations throughout the network (Fig. 6 *A*, *C*, and *E*) and no tremor frequency in the Vim spectrogram (Fig. 6*G*). Vice versa, under ET condition, we varied the number of ION neurons that received the initial perturbation, and we determined whether sustained oscillations throughout the network were elicited. The ION neurons receiving the perturbation were chosen among those interconnected by gap junctions. Across five instances of the scale-up model, we found that an initial perturbation delivered to ~50% of the ION neurons (average, 20.8 ± 5.4, mean ± SD; minimum, 16; maximum, 30) elicited a sustained spiking activity in the entire ION population within 500 ms (e.g., see example in Fig. 6*B*), along with complex spikes in the PCs and sustained bursting activity in the DCNs (Fig. 6 *D* and *F*). The resultant widespread network oscillation was then associated with a sustained tremor activity in the Vim (Fig. 6*H*).

Overall, the spread of tremor-related oscillations across multiple olivocerebellar loops indicates that under GABAergic dysfunction, the olivocerebellar system is highly susceptible to perturbations and can rapidly converge to global, tremor-related oscillatory dynamics.

Discussion

The cellular origins of ET have been intensively investigated over the past 20 y. The presence of tremor cells in the cerebellum-recipient regions of thalamus in ET patients (31) indicates that the cerebellothalamic pathway is pivotal to the generation of tremor. Moreover, ref. 58 reported an abnormal eyeblink conditioning in patients with ET, which suggests that the olivocerebellar system may be functionally impaired. Furthermore, studies (16, 59, 60) have reported several microstructural alterations in the cerebellar cortex of ET patients, including a diffused loss of the Purkinje cells, reduced dendritic arborizations, and axonal swellings, which may severely alter the cerebellar activity. Studies (17–19) have also reported a significant increment of $GABA_A$ receptor binding sites in the cerebellum and, locally, a significant decrease of $GABA_A$ and $GABA_B$ receptors in the dentate nucleus in ET patients. Finally, disorders that involve cerebellar dysfunction like motor learning impairment are frequently reported in ET subjects (61) along with a generalized hyperactivation of the cerebellar structures during movements (13, 62). Altogether, these results have contributed to the hypothesis that a cerebellar dysfunction may lead to pathologic activity along the cerebellothalamic pathway. It is unclear, though, how tremor-related activity in the Vim could result from such a variety of changes reported in the cerebellum. Our model provides a mechanistic explanation that reconciles several, apparently contradicting experimental observations. The following predictions are made.

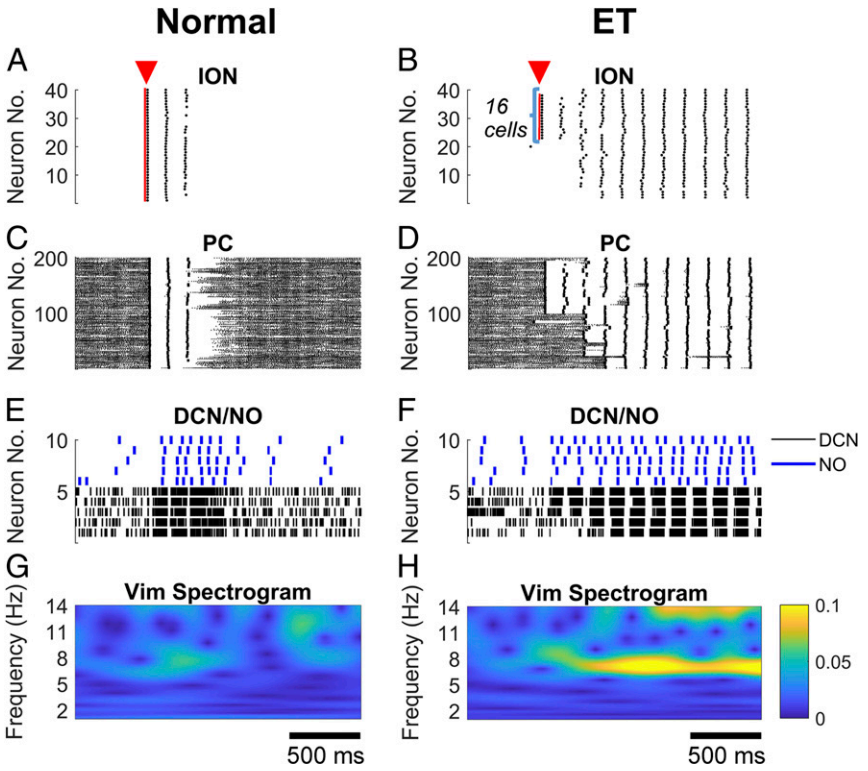

Fig. 6. Scale-up model (i.e., 425- instead of 85-single compartment model) under normal, tremor-free condition (*A*, *C*, *E*, and *G*) and ET condition (i.e., yellow circle in Fig. 3*A*) (*B*, *D*, *F*, and *H*), respectively. (*A*) A current pulse (duration, 20 ms; amplitude, 10 pA) was applied to all 40 ION neurons simultaneously (red triangle), which led to synchronous firing of ION neurons for 2–3 cycles but no tonic spiking activity. (*B*) The same current pulse as in *A* was applied to 16 ION neurons simultaneously under ET condition (red triangle) and caused tonic spiking activities that spread to the entire ION neuron population. (*C*–*F*) Spiking pattern of the PC, DCN, and NO neurons in response to the exogenous pulse to the ION neurons in *A* (*C* and *E*) and in *B* (*D* and *F*). (*G* and *H*) Power spectrogram of the Vim in response to the pulse to the ION neurons in *A* (*G*) and in *B* (*H*). Note that under ET condition, a prominent 7–8 Hz oscillation emerged in the spectrogram after the ION neurons were engaged into tonic spiking. Time scales in *G* and *H* also apply to *A*, *C*, and *E* and *B*, *D*, and *F*, respectively.

Tremor Oscillations May Have Network Origins. Studies (15, 20, 21, 63) have reported diffused alterations to the functional networks among cerebellum, thalamus, and cortices during motor tasks in ET subjects, including a significant reduction of the connectivity between cortical and cerebellar motor areas as well as between cerebellar cortex and dentate nuclei, and an increment in low-frequency oscillatory activity in the motor cortices. Both the reduction in connectivity and the increment in low-frequency oscillations positively correlated with the severity of kinetic tremor, thus suggesting a link between network dysfunctions and tremor. Although it is unclear how oscillations in the cerebellum affect the activity of the cerebral cortex, it has been suggested that the structural alterations in the cerebellum may alter the cerebellar output to the cortico-thalamo-cerebellar networks, thus contributing to the disruption of the connectivity in these functional networks (20).

Our study identifies a potential network-based mechanism to sustain and amplify tremor-related neural oscillations. We predict that such oscillations are sustained by the interplay between inferior olivary nucleus, dentate nucleus, and cerebellar cortex. The oscillatory activity propagates along the olivocerebellar pathway into the cerebellum and reenters the olivary nucleus through the dentato-rubro-olivary pathway. In addition, localized perturbations to a small portion of neurons in the inferior olive nucleus can initiate neural oscillations that quickly spread to a larger network and eventually alter the thalamocortical discharge patterns. This prediction reconciles the role of the inferior olivary nucleus in maintaining neural oscillations with the lack of olivary dysfunctions reported in ET patients (10–12) and suggests that the olivary neurons may be recruited into tremor oscillations via the dentato-rubro-olivary pathway because of their intrinsic pacemaker capabilities, with no need for specific alterations of the ion channels or synapses.

Although there is little knowledge about the dentato-rubro-olivary pathway, studies in ET patients have recently suggested that this pathway may be involved in tremor generation (64, 65). It is also known that drugs (e.g., alcohol) that interfere with the synaptic transmissions along this pathway can attenuate tremor symptoms and reduce the size of Purkinje cells' complex spikes following climbing fiber activation (66, 67). Our model predicts that the reduction in complex spikes would result in shorter hyperpolarization and weaker rebound firing of the deep cerebellar neurons and therefore cause a decreased activity of the dentato-rubro-olivary pathway, which is consistent with observations reported in ref. 66. We expect that the manipulation of this pathway in animal models, e.g., via optogenetic stimulation of the red nucleus, might help further assess the role in ET.

Slow-Decaying GABAergic Currents in the Dentate Nucleus Contribute to Sustained Neural Oscillations. It has been speculated that the loss of Purkinje cells and the structural changes to the cerebellar cortex may cause a reorganization of the Purkinje cell functional network as well as the interface between climbing fibers and Purkinje cells (2). This reorganization would result in a reduced GABAergic modulation of the dentate nuclei and a facilitation of the pacemaker activity of the DCN cells, which would eventually propagate to the thalamus (2). Our study suggests that a nonspecific reduction in the GABAergic currents to the DCN can increase its average firing rate and thus the glutamatergic input to the thalamus, but it does not lead to a rhythmic activity

in the tremor band either in the DCN or Vim. This is supported by the observation that deep cerebellar neurons rarely exhibit spontaneous pacemaker activity at frequencies within the tremor band (68). This is also consistent with earlier studies, e.g., ref. 69, which reported that the degeneration of Purkinje cells alone may be insufficient to elicit sustained oscillations in the Vim, while highly synchronized afferent currents from the deep cerebellar structures are required to recruit the thalamocortical neurons.

Our study suggests that the temporal dynamics of the GABAergic currents may be critical for tremor generation. Although none of the parametric changes that we applied to the GABAergic currents were sufficient to initiate tremor-related network oscillations in our model, we found that a specific range of GABAergic currents to the dentate nucleus can make these oscillations outlast the initial perturbation and self-sustain. This suggests that the role of the cerebellar dysfunctions in ET may be related to the preservation, amplification, and propagation of the tremor oscillations. Moreover, the need for an initial perturbation may be linked to the fact that tremor oscillations in the thalamus are enabled by voluntary movement, while absent at rest (31).

On the other hand, the preservation of network oscillations depends on the dynamics of the GABAergic currents. Specifically, the GABAergic dysfunctions between Purkinje cells and dentate neurons may reduce the fast α_1-subunit–mediated currents and increase the slowly decaying currents mediated by the up-regulated $\alpha_{2/3}$ subunits (23–26). Our model predicts that such currents can facilitate the after-hyperpolarization rebound of the deep cerebellar neurons, which robustly activates the olivary neurons at a preferred phase of their subthreshold oscillations, thus facilitating the synchronization along the olivocerebellar loop. Also, other ET-related pathologies such as the increased Purkinje cell axonal branching, recurrent collaterals, and terminal axonal sprouting may further amplify such synchronization and therefore exacerbate tremor symptoms, even with substantial losses of inferior olive neurons and Purkinje cells (70, 71).

Finally, our model shows that the range of tremor-related GABAergic currents to the dentate nucleus increases as the synaptic current from the nucleoolivary neurons to the inferior olivary nucleus (NO→ION) decreases. This is mediated by an increment of the connectivity between olivary neurons, which occurs because the modeled NO→ION pathway has an inhibitory effect on the gap junctions between olivary neurons. The net effect is consistent with the regulatory action of the NO→ION pathway on the neuronal coupling in the inferior olivary nucleus (72). However, the interaction between ION and NO neurons involves additional connections, such as the projections from climbing fibers to NO neurons (73), which are currently neglected in our model and may contribute a negative feedback to the ION neurons. In addition, the specific localization of the NO synapses on the ION neurons and the morphology of the dendrites of ION neurons may significantly steer the synchronization within the inferior olivary nucleus (72, 74–76). Accordingly, it is plausible that the NO–ION connectivity may affect the network oscillations. For instance, it is possible that the adaptation of the discharge pattern of NO and ION neurons may result in a wider range of oscillation frequencies across the entire network than in our model. Similarly, as the ION neurons form groups of densely coupled neurons interspersed with areas of weak coupling (75), it is possible that different circuits along the olivocerebellar pathway have oscillations at slightly different frequencies, thus resulting in a more complex spreading of the neural oscillations through the network.

Neurostimulation Modulates Tremor Networks. Currently, Vim DBS remains the most successful neurostimulation therapy for ET. We investigated the effects of Vim DBS on different structures in the CCTC model. Although our representation of DBS aimed to mimic the shift in discharge pattern in Vim (57) and therefore lacks explicit representation of other mechanisms (77), the local effects of Vim DBS on the thalamocortical and pyramidal neurons were consistent with recordings in ET subjects, showing a robust attenuation of the tremor oscillations in the Vim and activation of the motor cortex (78). Our results show that although the main effect of Vim DBS likely involves blocking tremor oscillations at thalamocortical level (77), through an increment in cortical excitability, it also has secondary effects on the neural oscillations in the olivocerebellar structures, which received a shift in frequency consistent with clinical observations (34, 56). It also provides an explanation for the higher tremor frequency in kinetic versus postural tasks since the former presumably involve a higher motor cortical activity (79). Altogether, these predictions suggest that the oscillations underlying ET may involve a large network including both the cerebellar and cerebral structures.

Materials and Methods

Computational Model. We developed a network of 85 single-compartment model neurons (73 biophysically based neurons and 12 leaky integrate-and-fire neurons). The equations and parameters for the model neurons of PC, GrL cluster, TC, PYN, and FSI were obtained from refs. 80–83, respectively, and modified as reported in *SI Appendix, Note 1*. The ION neuron included the soma compartment of the multicompartment model in ref. 48, with calcium channel equations from refs. 84 and 85, which account for the reduction to single-compartment and fit in vitro recordings from rodents reported in ref. 85. The DCN model neuron included the soma compartment of the multicompartment model in ref. 86, with ion channel conductance values adjusted to account for the reduction to single-compartment (*SI Appendix*, Table S1). The NO model neuron was derived from the DCN model and includes fast sodium channels, fast and slow delayed rectifier potassium channels, and leaky channels with parameters adjusted to match the in vitro recordings in ref. 54 as shown in *SI Appendix*, Fig. S2 *E–H* (model described in *SI Appendix, Note 1*). The ratios of PCs to DCN (40:1) and PYNs to FSIs (20:2) were as in refs. 87 and 88, respectively, and account for the convergence of PCs onto DCNs, as well as the extensive connectivity of the cortical pyramidal neurons and interneurons. Details about the network connectivity are reported in *SI Appendix, Note 1* and Fig. S3.

Each neuron was endowed with a constant current (I_{OC}) to simulate the background excitation and a Gaussian noise with zero mean to simulate the subthreshold membrane voltage fluctuations (±5 mV). The intensity of current I_{OC} varied across the ION neurons (uniform distribution) to generate subthreshold oscillations at different frequencies. Similarly, the intensity of I_{OC} varied across the PCs (gamma distribution) to simulate a range of spontaneous firing rates. See values in *SI Appendix*, Tables S1 and S2. The transition from normal conditions to harmaline-induced tremor conditions was simulated by modifying the ION model neuron as proposed in ref. 48. Briefly, the maximum conductance of the ION calcium channels was increased from 0.27 to 0.3 mS•cm^2 and the maximum conductance of h-type channels was lowered from 0.08 to 0.02 mS•cm^2 to mimic the experimental conditions reported in ref (6), while the intensity of I_{OC} was set to 2 pA for all ION neurons. Accordingly, all ION neurons presented subthreshold oscillations at the same frequency and became spontaneously active, with one action potential fired by each neuron in synchrony per oscillation cycle.

Computational Tools. In each analysis, three different instances of the model network were generated. Numerical simulations were programmed in NEURON, ver. 7.5 (89), and run on an eight-core Intel Xeon workstation (3.6 GHz/core, 16 GB RAM). The differential equations were integrated via CVODE method with time step 0.0125 ms. Results were analyzed in MATLAB R2017a (The MathWorks, Inc.). We implemented published algorithms to compute firing and burst rates, power spectral densities, and cross-correlation as in refs. 90 and 91. Further details about the implementation are given in *SI Appendix, Note 2*. The NEURON code implementing the proposed model is available on ModelDB (http://modeldb.yale.edu/257028).

ACKNOWLEDGMENTS. This work was partly supported by the Connecticut Institute for the Brain and Cognitive Sciences IBRAiN Fellowship (to X.Z.) and the US National Science Foundation CAREER Award 1845348 (to S.S.).

1. E. D. Louis, J. J. Ferreira, How common is the most common adult movement disorder? Update on the worldwide prevalence of essential tremor. *Mov. Disord.* **25**, 534–541 (2010).
2. E. D. Louis, Essential tremor and the cerebellum. *Handb. Clin. Neurol.* **155**, 245–258 (2018).
3. K. P. Bhatia *et al*.; Tremor Task Force of the International Parkinson and Movement Disorder Society, Consensus statement on the classification of tremors. From the task force on tremor of the International Parkinson and Movement Disorder Society. *Mov. Disord.* **33**, 75–87 (2018).
4. K. E. Lyons, R. Pahwa, Deep brain stimulation and essential tremor. *J. Clin. Neurophysiol.* **21**, 2–5 (2004).
5. M. R. DeLong, Possible involvement of central pacemakers in clinical disorders of movement. *Fed. Proc.* **37**, 2171–2175 (1978).
6. Y. G. Park *et al*., Ca(V)3.1 is a tremor rhythm pacemaker in the inferior olive. *Proc. Natl. Acad. Sci. U.S.A.* **107**, 10731–10736 (2010).
7. R. Llinás, Y. Yarom, Electrophysiology of mammalian inferior olivary neurones in vitro. Different types of voltage-dependent ionic conductances. *J. Physiol.* **315**, 549–567 (1981).
8. Y. Lamarre, L. A. Mercier, Neurophysiological studies of harmaline-induced tremor in the cat. *Can. J. Physiol. Pharmacol.* **49**, 1049–1058 (1971).
9. R. Llinás, R. A. Volkind, The olivo-cerebellar system: Functional properties as revealed by harmaline-induced tremor. *Exp. Brain Res.* **18**, 69–87 (1973).
10. E. D. Louis, R. Babij, E. Cortés, J. P. Vonsattel, P. L. Faust, The inferior olivary nucleus: A postmortem study of essential tremor cases versus controls. *Mov. Disord.* **28**, 779–786 (2013).
11. S. F. Bucher, K. C. Seelos, R. C. Dodel, M. Reiser, W. H. Oertel, Activation mapping in essential tremor with functional magnetic resonance imaging. *Ann. Neurol.* **41**, 32–40 (1997).
12. M. Hallett, R. M. Dubinsky, Glucose metabolism in the brain of patients with essential tremor. *J. Neurol. Sci.* **114**, 45–48 (1993).
13. F. L. Pagan, J. A. Butman, J. M. Dambrosia, M. Hallett, Evaluation of essential tremor with multi-voxel magnetic resonance spectroscopy. *Neurology* **60**, 1344–1347 (2003).
14. A. J. Wills, I. H. Jenkins, P. D. Thompson, L. J. Findley, D. J. Brooks, A positron emission tomography study of cerebral activation associated with essential and writing tremor. *Arch. Neurol.* **52**, 299–305 (1995).
15. W. Yin, W. Lin, W. Li, S. Qian, X. Mou, Resting state fMRI demonstrates a disturbance of the cerebello-cortical circuit in essential tremor. *Brain Topogr.* **29**, 412–418 (2016).
16. E. D. Louis *et al*., Reduced Purkinje cell dendritic arborization and loss of dendritic spines in essential tremor. *Brain* **137**, 3142–3148 (2014).
17. S. Paris-Robidas *et al*., Defective dentate nucleus GABA receptors in essential tremor. *Brain* **135**, 105–116 (2012).
18. H. Boecker *et al*., GABAergic dysfunction in essential tremor: An 11C-flumazenil PET study. *J. Nucl. Med.* **51**, 1030–1035 (2010).
19. A. Gironell *et al*., Gaba and serotonin molecular neuroimaging in essential tremor: A clinical correlation study. *Parkinsonism Relat. Disord.* **18**, 876–880 (2012).
20. A. W. Buijink *et al*., Motor network disruption in essential tremor: A functional and effective connectivity study. *Brain* **138**, 2934–2947 (2015).
21. C. Gallea *et al*., Intrinsic signature of essential tremor in the cerebello-frontal network. *Brain* **138**, 2920–2933 (2015).
22. J. E. Kralic *et al*., Genetic essential tremor in gamma-aminobutyric acidA receptor alpha1 subunit knockout mice. *J. Clin. Invest.* **115**, 774–779 (2005).
23. J. E. Kralic, E. R. Korpi, T. K. O'Buckley, G. E. Homanics, A. L. Morrow, Molecular and pharmacological characterization of GABA(A) receptor alpha1 subunit knockout mice. *J. Pharmacol. Exp. Ther.* **302**, 1037–1045 (2002).
24. J. M. Fritschy, P. Panzanelli, Molecular and synaptic organization of GABAA receptors in the cerebellum: Effects of targeted subunit gene deletions. *Cerebellum* **5**, 275–285 (2006).
25. T. Stojanovic *et al*., The α1, α2, α3, and γ2 subunits of GABAA receptors show characteristic spatial and temporal expression patterns in rhombencephalic structures during normal human brain development. *J. Comp. Neurol.* **524**, 1805–1824 (2016).
26. J. E. Kralic *et al*., Compensatory alteration of inhibitory synaptic circuits in cerebellum and thalamus of gamma-aminobutyric acid type A receptor alpha1 subunit knockout mice. *J. Comp. Neurol.* **495**, 408–421 (2006).
27. P. I. Ortinski, C. Lu, K. Takagaki, Z. Fu, S. Vicini, Expression of distinct alpha subunits of GABAA receptor regulates inhibitory synaptic strength. *J. Neurophysiol.* **92**, 1718–1727 (2004).
28. C. Dixon, P. Sah, J. W. Lynch, A. Keramidas, GABAA receptor α and γ subunits shape synaptic currents via different mechanisms. *J. Biol. Chem.* **289**, 5399–5411 (2014).
29. E. Ramadan *et al*., GABA(A) receptor beta3 subunit deletion decreases alpha2/3 subunits and IPSC duration. *J. Neurophysiol.* **89**, 128–134 (2003).
30. P. I. Ortinski *et al*., Deletion of the GABA(A) receptor alpha1 subunit increases tonic GABA(A) receptor current: A role for GABA uptake transporters. *J. Neurosci.* **26**, 9323–9331 (2006).
31. S. E. Hua, F. A. Lenz, Posture-related oscillations in human cerebellar thalamus in essential tremor are enabled by voluntary motor circuits. *J. Neurophysiol.* **93**, 117–127 (2005).
32. H. Chen *et al*., Neuronal firing in the ventrolateral thalamus of patients with Parkinson's disease differs from that with essential tremor. *Chin. Med. J. (Engl.)* **123**, 695–701 (2010).
33. R. J. Elble, Essential tremor frequency decreases with time. *Neurology* **55**, 1547–1551 (2000).
34. D. E. Vaillancourt, M. M. Sturman, L. Verhagen Metman, R. A. Bakay, D. M. Corcos, Deep brain stimulation of the VIM thalamic nucleus modifies several features of essential tremor. *Neurology* **61**, 919–925 (2003).
35. W. T. Thach, Discharge of Purkinje and cerebellar nuclear neurons during rapidly alternating arm movements in the monkey. *J. Neurophysiol.* **31**, 785–797 (1968).
36. R. Ashida, N. L. Cerminara, J. Brooks, R. Apps, Principles of organization of the human cerebellum: Macro- and microanatomy. *Handb. Clin. Neurol.* **154**, 45–58 (2018).
37. P. Bazzigaluppi, T. Ruigrok, P. Saisan, C. I. De Zeeuw, M. de Jeu, Properties of the nucleo-olivary pathway: An in vivo whole-cell patch clamp study. *PLoS One* **7**, e46360 (2012).
38. T. J. Ruigrok, J. Voogd, Cerebellar influence on olivary excitability in the cat. *Eur. J. Neurosci.* **7**, 679–693 (1995).
39. H. Oka, K. Jinnai, Electrophysiological study of parvocellular red nucleus neurons. *Brain Res.* **149**, 239–246 (1978).
40. K. Sasaki, S. Kawaguchi, T. Shimono, S. Prelević, Electrophysiological studies of the pontine nuclei. *Brain Res.* **20**, 425–438 (1970).
41. F. Palesi *et al*., Contralateral cortico-ponto-cerebellar pathways reconstruction in humans in vivo: Implications for reciprocal cerebro-cerebellar structural connectivity in motor and non-motor areas. *Sci. Rep.* **7**, 12841 (2017).
42. B. Pasquereau, M. R. DeLong, R. S. Turner, Primary motor cortex of the parkinsonian monkey: Altered encoding of active movement. *Brain* **139**, 127–143 (2016).
43. A. Mathy *et al*., Encoding of oscillations by axonal bursts in inferior olive neurons. *Neuron* **62**, 388–399 (2009).
44. C. Hansel, D. J. Linden, Long-term depression of the cerebellar climbing fiber–Purkinje neuron synapse. *Neuron* **26**, 473–482 (2000).
45. F. Bengtsson, C. F. Ekerot, H. Jörntell, In vivo analysis of inhibitory synaptic inputs and rebounds in deep cerebellar nuclear neurons. *PLoS One* **6**, e18822 (2011).
46. F. E. Hoebeek, L. Witter, T. J. Ruigrok, C. I. De Zeeuw, Differential olivo-cerebellar cortical control of rebound activity in the cerebellar nuclei. *Proc. Natl. Acad. Sci. U.S.A.* **107**, 8410–8415 (2010).
47. E. Chorev, Y. Yarom, I. Lampl, Rhythmic episodes of subthreshold membrane potential oscillations in the rat inferior olive nuclei in vivo. *J. Neurosci.* **27**, 5043–5052 (2007).
48. N. Schweighofer, K. Doya, M. Kawato, Electrophysiological properties of inferior olive neurons: A compartmental model. *J. Neurophysiol.* **82**, 804–817 (1999).
49. K. M. Horn, P. L. Van Kan, A. R. Gibson, Reduction of rostral dorsal accessory olive responses during reaching. *J. Neurophysiol.* **76**, 4140–4151 (1996).
50. A. R. Gibson, K. M. Horn, M. Pong, Activation of climbing fibers. *Cerebellum* **3**, 212–221 (2004).
51. C. Ohye *et al*., Effect of dorsal rhizotomy on postural tremor in the monkey. *Exp. Brain Res.* **10**, 140–150 (1970).
52. M. D. Eyre, M. Renzi, M. Farrant, Z. Nusser, Setting the time course of inhibitory synaptic currents by mixing multiple GABA(A) receptor α subunit isoforms. *J. Neurosci.* **32**, 5853–5867 (2012).
53. M. Uusisaari, T. Knöpfel, GABAergic synaptic communication in the GABAergic and non-GABAergic cells in the deep cerebellar nuclei. *Neuroscience* **156**, 537–549 (2008).
54. M. Najac, I. M. Raman, Integration of Purkinje cell inhibition by cerebellar nucleo-olivary neurons. *J. Neurosci.* **35**, 544–549 (2015).
55. K. Zhang *et al*., Long-term results of thalamic deep brain stimulation for essential tremor. *J. Neurosurg.* **112**, 1271–1276 (2010).
56. K. M. Zackowski *et al*., Thalamic stimulation reduces essential tremor but not the delayed antagonist muscle timing. *Neurology* **58**, 402–410 (2002).
57. A. M. Kuncel, S. E. Cooper, B. R. Wolgamuth, W. M. Grill, Amplitude- and frequency-dependent changes in neuronal regularity parallel changes in tremor with thalamic deep brain stimulation. *IEEE Trans. Neural Syst. Rehabil. Eng.* **15**, 190–197 (2007).
58. M. Kronenbuerger, M. Gerwig, B. Brol, F. Block, D. Timmann, Eyeblink conditioning is impaired in subjects with essential tremor. *Brain* **130**, 1538–1551 (2007).
59. E. D. Louis *et al*., Neuropathological changes in essential tremor: 33 cases compared with 21 controls. *Brain* **130**, 3297–3307 (2007).
60. M. Choe *et al*., Purkinje cell loss in essential tremor: Random sampling quantification and nearest neighbor analysis. *Mov. Disord.* **31**, 393–401 (2016).
61. P. Trillenberg *et al*., Eye-hand coordination in essential tremor. *Mov. Disord.* **21**, 373–379 (2006).
62. A. J. Wills, I. H. Jenkins, P. D. Thompson, L. J. Findley, D. J. Brooks, Red nuclear and cerebellar but no olivary activation associated with essential tremor: A positron emission tomographic study. *Ann. Neurol.* **36**, 636–642 (1994).
63. K. J. Petersen *et al*., Structural and functional connectivity of the nondecussating dentato-rubro-thalamic tract. *Neuroimage* **176**, 364–371 (2018).
64. A. Schnitzler, C. Münks, M. Butz, L. Timmermann, J. Gross, Synchronized brain network associated with essential tremor as revealed by magnetoencephalography. *Mov. Disord.* **24**, 1629–1635 (2009).
65. M. Muthuraman *et al*., Oscillating central motor networks in pathological tremors and voluntary movements. What makes the difference? *Neuroimage* **60**, 1331–1339 (2012).
66. H. Boecker *et al*., The effect of ethanol on alcohol-responsive essential tremor: A positron emission tomography study. *Ann. Neurol.* **39**, 650–658 (1996).
67. M. Carta, M. Mameli, C. F. Valenzuela, Alcohol potently modulates climbing fiber–>Purkinje neuron synapses: Role of metabotropic glutamate receptors. *J. Neurosci.* **26**, 1906–1912 (2006).
68. D. Pinault, M. Deschênes, The origin of rhythmic fast subthreshold depolarizations in thalamic relay cells of rats under urethane anaesthesia. *Brain Res.* **595**, 295–300 (1992).
69. S. Roffler-Tarlov, P. M. Beart, S. O'Gorman, R. L. Sidman, Neurochemical and morphological consequences of axon terminal degeneration in cerebellar deep nuclei of mice with inherited Purkinje cell degeneration. *Brain Res.* **168**, 75–95 (1979).
70. R. Babij *et al*., Purkinje cell axonal anatomy: Quantifying morphometric changes in essential tremor versus control brains. *Brain* **136**, 3051–3061 (2013).

71. E. D. Louis *et al*., Inferior Olivary nucleus degeneration does not lessen tremor in essential tremor. *Cerebellum Ataxias* **5**, 1 (2018).
72. Y. Lefler, Y. Yarom, M. Y. Uusisaari, Cerebellar inhibitory input to the inferior olive decreases electrical coupling and blocks subthreshold oscillations. *Neuron* **81**, 1389–1400 (2014).
73. V. Chan-Palay, On the identification of the afferent axon terminals in the nucleus lateralis of the cerebellum. An electron microscope study. *Z. Anat. Entwicklungsgesch.* **142**, 149–186 (1973).
74. V. Chan-Palay, Axon terminals of the intrinsic neurons in the nucleus lateralis of the cerebellum. An electron microscope study. *Z. Anat. Entwicklungsgesch.* **142**, 187–206 (1973).
75. N. Vrieler *et al*., Variability and directionality of inferior olive neuron dendrites revealed by detailed 3D characterization of an extensive morphological library. *Brain Struct. Funct.* **224**, 1677–1695 (2019).
76. M. Uusisaari, T. Knöpfel, Functional classification of neurons in the mouse lateral cerebellar nuclei. *Cerebellum* **10**, 637–646 (2011).
77. L. Milosevic *et al*., Physiological mechanisms of thalamic ventral intermediate nucleus stimulation for tremor suppression. *Brain* **141**, 2142–2155 (2018).
78. G. F. Molnar *et al*., Changes in cortical excitability with thalamic deep brain stimulation. *Neurology* **64**, 1913–1919 (2005).
79. N. Schuhmayer *et al*., Task-dependent variability of essential tremor. *Parkinsonism Relat. Disord.* **41**, 79–85 (2017).
80. W. Akemann, T. Knöpfel, Interaction of Kv3 potassium channels and resurgent sodium current influences the rate of spontaneous firing of Purkinje neurons. *J. Neurosci.* **26**, 4602–4612 (2006).
81. J. A. Garrido, E. Ros, E. D'Angelo, Spike timing regulation on the millisecond scale by distributed synaptic plasticity at the cerebellum input stage: A simulation study. *Front. Comput. Neurosci.* **7**, 64 (2013).
82. H. G. Meijer *et al*., From Parkinsonian thalamic activity to restoring thalamic relay using deep brain stimulation: New insights from computational modeling. *J. Neural Eng.* **8**, 066005 (2011).
83. A. Destexhe, D. Contreras, M. Steriade, Mechanisms underlying the synchronizing action of corticothalamic feedback through inhibition of thalamic relay cells. *J. Neurophysiol.* **79**, 999–1016 (1998).
84. Y. Manor, J. Rinzel, I. Segev, Y. Yarom, Low-amplitude oscillations in the inferior olive: A model based on electrical coupling of neurons with heterogeneous channel densities. *J. Neurophysiol.* **77**, 2736–2752 (1997).
85. B. Torben-Nielsen, I. Segev, Y. Yarom, The generation of phase differences and frequency changes in a network model of inferior olive subthreshold oscillations. *PLoS Comput. Biol.* **8**, e1002580 (2012).
86. V. Steuber, N. W. Schultheiss, R. A. Silver, E. De Schutter, D. Jaeger, Determinants of synaptic integration and heterogeneity in rebound firing explored with data-driven models of deep cerebellar nucleus cells. *J. Comput. Neurosci.* **30**, 633–658 (2011).
87. A. L. Person, I. M. Raman, Purkinje neuron synchrony elicits time-locked spiking in the cerebellar nuclei. *Nature* **481**, 502–505 (2011).
88. M. M. McCarthy, E. N. Brown, N. Kopell, Potential network mechanisms mediating electroencephalographic beta rhythm changes during propofol-induced paradoxical excitation. *J. Neurosci.* **28**, 13488–13504 (2008).
89. N. T. Carnevale, M. L. Hines, *The Neuron Book* (Cambridge University Press, Cambridge, UK, 2006), 457 pp.
90. S. Santaniello *et al*., Therapeutic mechanisms of high-frequency stimulation in Parkinson's disease and neural restoration via loop-based reinforcement. *Proc. Natl. Acad. Sci. U.S.A.* **112**, E586–E595 (2015).
91. D. J. Bakkum *et al*., Parameters for burst detection. *Front. Comput. Neurosci.* **7**, 193 (2014).